

Flows through plane sudden-expansions

S. R. N. De Zilwa^a, L. Khezzar^b and J. H. Whitelaw^{a,*}

^a *Mechanical Engineering Department, Imperial College of Science Technology and Medicine, London, UK*

^b *College of Engineering, Sultan Qaboos University, Muscat, Oman*

SUMMARY

A calculation method has been developed and used to represent flows downstream of plane symmetric expansions with dimensions and velocities encompassing laminar and turbulent flows. Except for very low Reynolds numbers, the flows are time-dependent and asymmetric and the calculated results are appraised first in relation to published measurements of laminar flows and then to new measurements obtained at a Reynolds number of 26500. The time-dependent laminar simulations indicate that the critical Reynolds numbers are predicted with excellent accuracy for different expansion ratios and the details of the asymmetric velocity profiles are in good agreement with experimental measurements. The laminar flow calculations also show that increasing the thickness of the separating boundary layer leads to longer regions of separation and no dominant frequency for Reynolds numbers up to those at which the third separation region was observed. The turbulent flow simulations made use of the $k-\varepsilon$ turbulence model and provided a satisfactory representation of measurements, except in regions close to the wall and within the recirculation regions. Also, the longer reattachment length was underestimated. Limitations are discussed in relation to these and higher-order assumptions. Copyright © 2000 John Wiley & Sons, Ltd.

KEY WORDS: laminar flow; Reynolds number; sudden expansions; turbulent flow

1. INTRODUCTION

At sufficiently low values of the Reynolds number based on the upstream duct height and its centreline velocity, the flow downstream of a plane symmetric sudden-expansion is symmetric and becomes asymmetric as the Reynolds number is increased beyond a critical value, with the appearance of two and, subsequently, three recirculation zones at higher laminar flow Reynolds numbers. It is known that turbulent flows also give rise to asymmetric flows. Understanding these flows is relevant to several important engineering applications, including fluidic devices, heat exchangers, mixing equipment, flame holders in combustion systems and

* Correspondence to: Mechanical Engineering Department, Imperial College of Science Technology and Medicine, Exhibition Road, London, SW7 2BX, UK. Tel.: +44 171 5747028/9; fax: +44 171 5893905/8238845; e-mail: j.whitelaw@ic.ac.uk

channel flows. The present results are one part of an investigation of plane sudden-expansion flows that involves combustion with and without major acoustic effects.

Experimental investigations of plane sudden-expansion flows have been reported by Durst *et al.* [1], Cherdron *et al.* [2] and Fearn *et al.* [3], who used laser-Doppler anemometry to measure the velocity distributions, including those in close proximity of the recirculation regions, and flow visualization to show the nature of laminar flows. Two recirculation zones were identified in [1], and a third in [2], which was quantified in terms of detailed velocity measurements [3]. Shedding of time-dependent vortex-like patterns was observed by these authors at modestly high Reynolds numbers and was associated with the third recirculation zone. The exact nature of these unsteady features is incompletely understood, but it was conjectured notably by Fearn *et al.* [3] on the basis of visual observations that they are a consequence of three-dimensional effects in the channel. Ouwa *et al.* [4] suggested that the unsteady shedding was a prelude to the disappearance of the third recirculation zone as the Reynolds number is increased in this transitional regime. Limited investigations of turbulent flows have been reported by Abbot and Kline [5], Restivo and Whitelaw [6] and Mehta [7], who used flow visualization by tufts, laser-Doppler anemometry and a Pitot tube, respectively. They confirmed the asymmetry of high-Reynolds number flows with two unequal regions of recirculation in all cases. High-Reynolds number, two-phase bubbly flows through plane symmetric-expansions were examined by Aloui and Sonhar [8], and were symmetric with void fractions above 10% although the accuracy of measurement was less than in single-phase flows. Also, as part of the present investigations, early experiments have shown that asymmetry is considerably reduced by combustion.

Numerical investigations include those of Fearn *et al.* [3], Durst *et al.* [9], Battaglia *et al.* [10], Gagnon *et al.* [11] and Mizushima *et al.* [12] and made use of conventional time marching finite difference and element integration techniques with primitive Navier–Stokes and vorticity–streamfunction formulations, bifurcation analysis and random vortex methods; with the time-dependent nature of the flow considered in all cases. Except for [11], they focused on laminar flows and the main conclusion was that the flow through a plane symmetric sudden-expansion becomes unstable as the Reynolds number is increased above a critical value, to yield a stable and asymmetric solutions through a pitchfork (symmetry breaking) bifurcation. There is evidence that transition occurs smoothly and it has been established that the critical Reynolds number decreases with expansion ratio and is affected by the aspect ratio. Foumeny *et al.* [13] investigated the critical Reynolds number for a plane symmetric-expansion and for parallel multi-channel cascade systems that are relevant to mixing equipment and found that it was lower for the latter configuration. Alleborn *et al.* [14] reported a second bifurcation at a higher Reynolds number and, in contrast to the first bifurcation, the asymmetric solutions arising from the second bifurcation point were unstable with the implication that two-dimensional flows cannot exist.

The main purpose of this paper is to describe, evaluate and apply a calculation method, based on the solution of unsteady forms of the conservation equations, to plane sudden-expansion flows. The evaluation is based on published velocity results for laminar flow, and particularly those of [3], since they provide details of recirculating flows, and on new velocity measurements for a turbulent flow and supported by visualization. The results include consideration of the critical Reynolds number, the length of the recirculation regions and the effects of expansion ratio and the shape of the initial velocity profile.

The velocity characteristics with expansion and aspect ratios of 2.86 and 4 respectively, were measured by laser-Doppler anemometry and correspond to a Reynolds number of 26500. The flow was visualized in terms of smoke for low Reynolds numbers and surface dye and pigment at high Reynolds numbers.

The numerical and experimental methods are described in the following two sections, with the latter providing a description of the flow configuration and boundary conditions. Section 4 presents an evaluation of the calculation methods in terms of measured laminar and turbulent flows and this was made possible in the latter case by the new measurements. The final two sections provide calculated flow properties outside the range of experimental boundary conditions and a summary of the more important conclusions.

2. NUMERICAL METHOD

The flow is assumed to be two-dimensional and time-dependent, the fluid viscous and incompressible, and with these assumptions, the continuity and momentum equations may be written in Cartesian co-ordinates as

$$\frac{\partial U}{\partial x} + \frac{\partial V}{\partial y} = 0, \tag{1}$$

$$\frac{\partial(\rho U)}{\partial t} + \frac{\partial(\rho U^2)}{\partial x} + \frac{\partial(\rho UV)}{\partial y} = -\frac{\partial P}{\partial x} + (\mu + \mu_t)\left(\frac{\partial^2 U}{\partial x^2} + \frac{\partial^2 U}{\partial y^2}\right), \tag{2}$$

$$\frac{\partial(\rho V)}{\partial t} + \frac{\partial(\rho UV)}{\partial x} + \frac{\partial(\rho V^2)}{\partial y} = -\frac{\partial P}{\partial y} + (\mu + \mu_t)\left(\frac{\partial^2 V}{\partial x^2} + \frac{\partial^2 V}{\partial y^2}\right), \tag{3}$$

where P represents the pressure and ρ and μ the density and viscosity of the fluid respectively. These equations apply to laminar and turbulent flows with the turbulent viscosity zero for the former and the dependent variable considered as ensemble-averages in the latter. The turbulent viscosity was represented here by the $k-\varepsilon$ model, which implies the need to solve two additional equations, namely

$$\frac{\partial(\rho k)}{\partial t} + \frac{\partial(\rho Uk)}{\partial x} + \frac{\partial(\rho Vk)}{\partial y} = \frac{\partial}{\partial x}\left(\frac{\mu_t}{\sigma_k} \frac{\partial k}{\partial x}\right) + \frac{\partial}{\partial y}\left(\frac{\mu_t}{\sigma_k} \frac{\partial k}{\partial y}\right) + G - \rho\varepsilon, \tag{4}$$

where

$$G = 2\mu_t \left[\left(\frac{\partial U}{\partial x}\right)^2 + \left(\frac{\partial V}{\partial y}\right)^2 + \frac{1}{2} \left(\frac{\partial U}{\partial x} + \frac{\partial V}{\partial y}\right)^2 \right],$$

$$\frac{\partial(\rho\varepsilon)}{\partial t} + \frac{\partial(\rho U\varepsilon)}{\partial x} + \frac{\partial(\rho V\varepsilon)}{\partial y} = \frac{\partial}{\partial x}\left(\frac{\mu_t}{\sigma_\varepsilon} \frac{\partial \varepsilon}{\partial x}\right) + \frac{\partial}{\partial y}\left(\frac{\mu_t}{\sigma_\varepsilon} \frac{\partial \varepsilon}{\partial y}\right) + \frac{\varepsilon}{k} (C_{1\varepsilon}G - C_{2\varepsilon}\rho\varepsilon), \tag{5}$$

the turbulent viscosity is given by

$$\mu_t = \rho C_\mu \frac{k^2}{\varepsilon}, \quad (6)$$

and the model constants are given in Table I.

The k - ε turbulence model assumes isotropic normal stresses and a single length scale to characterize the spectrum of turbulent motions. It also implies that the time dependence represented by the conservation equations encompasses a comparatively low-frequency range of the turbulent spectrum and omits consideration of the representation of this unsteadiness within the model. These are substantial assumptions but the approach is known to provide a good balance between accuracy and complexity. It can be expected to be less representative in regions of high streamline curvature and implies the need for wall functions to link the wall to the first grid node of the numerical methods described below.

The conservation equations were discretized by the third-order scheme of Leonard [15], a second-order centred difference scheme was adopted for diffusive fluxes and the pressure field was solved with the pressure implicit with splitting of operators (PISO) algorithm of Issa [16]. The quadratic upstream-weighted interpolation (QUICK) scheme being third-order-accurate possesses greater formal accuracy than the central or hybrid schemes and is considerably less prone to numerical diffusion and is known to return fairly accurate solutions. Temporal integration was achieved through a fully implicit formulation of Richtmeyer and Morton [17] and convergence was assumed when the global rates of change of the all variables were between 10^{-10} and 10^{-11} for laminar flow and less than 10^{-7} for turbulent flow. All the calculations were carried on a SUN-20 workstation to 64-bits precision and required in general around 30 h of CPU time.

The computational grid was rectangular and extended from the exit plane of the expansion to a position 70 and 50 step heights downstream for the turbulent and laminar cases respectively, with uniform distributions in the streamwise and cross-stream directions. Calculations were performed with grids corresponding to 150×55 and 200×93 and 250×110 nodes and, with no differences between the results with the last two grids, the intermediate grid was adopted for all production calculations.

The calculations proceeded by impulsively starting the flow from rest. At the inlet boundary, parabolic profiles were prescribed for the laminar flows of Section 4 and the measured axial velocity profile for the turbulent flow with turbulent kinetic energy and its rate of dissipation specified on the basis of 3% turbulent intensity, thus

$$k = 0.03 U_0^2, \quad \varepsilon = \frac{0.09 k^{3/2}}{h}. \quad (7)$$

Table I. Turbulence model constants

$\sigma_k = 1.0$	$\sigma_\varepsilon = 1.3$	$C_\mu = 0.09$	$C_{\varepsilon 1} = 1.44$	$C_{\varepsilon 2} = 1.92$
------------------	----------------------------	----------------	----------------------------	----------------------------

Zero axial gradients were assumed for all variables at a downstream boundary 0.7 m from the end of the expansion plane and a form of the law of the wall linked the zero velocity boundary condition to the first grid node from the wall.

It is known that the near-wall flow behaves like a laminar flow inside the recirculation region and in the recovery region, the velocity profile is below the universal log-law of the wall, see Le *et al.* [18]. Its use does, however, obviate the need to use an excessively fine grid near the wall as required by two-layer models and the resulting errors are expected to be local and to have little effect on the present results.

3. EXPERIMENTS

The flow arrangement of Figure 1 comprised a 51 mm internal diameter pipe followed by a transition section from circular to rectangular cross-section of 300 mm in length. A flow straightener was placed at the end of the transition duct and was followed by a duct of length 300 mm and 160 × 20 mm cross-section and a pair of ramps, which increased the step heights to 13 mm. It then expanded into a downstream rectangular duct of 160 × 40 mm, providing an area expansion ratio of 2.86. Some visualization results were obtained without the ramps. The length of this downstream section was 500 mm. A compressor supplied the air to the 51 mm diameter pipe (Figure 1) at a rate monitored by calibrated rotameters to a precision of 1%.

Visualization was achieved by introducing smoke at the base of the steps with illumination by a 1 kW lamp in a plane orthogonal to the expansion and photographing the illuminated smoke with a shutter speed of 1/30 s and an aperture of $f/2.8$. With higher Reynolds numbers, with which the smoke dispersed quickly, a thin metal sheet coated with pigment and light oil was introduced on the symmetry plane and the image formed by the drag of the pigment photographed with a shutter speed of 1/125 s and $f/1.8$.

The turbulent flow velocity was measured with a dual-beam laser-Doppler anemometer operated with light scattered in the forward direction from droplets of silicone oil with a mean diameter of 3 μm . A 15 mW He-Ne laser provided the coherent light source, the front lens had a focal length of 150 mm and the collimating and focussing lenses had focal lengths of 200

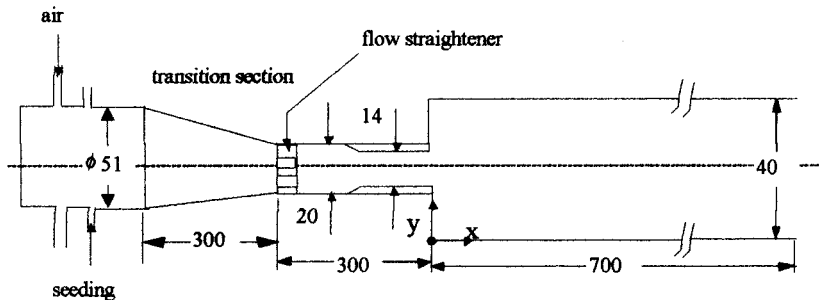


Figure 1. Geometry of the flow arrangement.

and 300 mm respectively. A rotating diffraction grating provided frequency shifts up to 2 MHz and the optical system was positioned on a milling table to allow translation in three orthogonal directions with a precision of 0.1 mm. The photomultiplier output was processed by a counter (TSI model 1990C), which was interfaced to a PC using a DMA interface card. The filtered and pre-amplified Doppler signal was monitored on an oscilloscope during the experiments.

Ensemble averages were formed from not less than 2500 velocity values with maximum statistical uncertainties of 1.9% in the mean velocity and 3% in the root-mean-square (r.m.s) velocity for a 95% confidence level, see Yanta and Smith [19]. Velocity gradient broadening was important only in regions of high velocity gradients and was minimized by the frequency shift, off-axis collection and a small pinhole on the photomultiplier, see Durst *et al.* [20]. The uncertainty in the mean and r.m.s velocities is estimated to be less than 3% and 6% respectively.

4. RESULTS

4.1. Experiments

The results of experiments are considered first since they provide the basis for evaluation of the numerical methods as well as providing new information. The laminar flow results of Fearn *et al.* [3] are preferred for the evaluation of laminar flows since they provide the greatest detail of the recirculation regions and are complemented here by visualization photographs to provide immediate confirmation of asymmetric flows. The present measurements provide the only detailed basis for comparison with turbulent flows and the following paragraphs describe sample visualization photographs and detailed velocities.

The two photographs of Figure 2 correspond to Reynolds numbers of 600 and 20000 and to the visualization of smoke and the drag of a pigment. They encompass identical areas of flow and are skewed towards the upper wall. The undulation of the flow is readily recognized in the flow at the lower Reynolds number with an upper dividing streamline, which has almost reattached, and a lower dividing streamline that is far from reattachment. Reattachment is less readily identified by the movement of the pigment, which tends to average the turbulent flow but is time-dependent with camera resolution of better than 100 Hz. It should be noted that the smaller region of recirculation occurred equally on the top and bottom step over many starts.

The measured velocities are presented in terms of profiles of the mean axial velocity and its corresponding r.m.s. of related fluctuations, with the co-ordinates of Figure 1 and normalization by the upstream centreline velocity. They correspond to a Reynolds number of 26500 based on the centreline velocity and duct height in the expansion plane. Figure 3(a) shows that the inlet flow had a near-uniform velocity of 21 m s^{-1} and turbulence intensity of 0.04. The inlet flow distribution in the spanwise direction was examined and confirmed that the flow was two-dimensional at the inlet, with the integration of the inlet

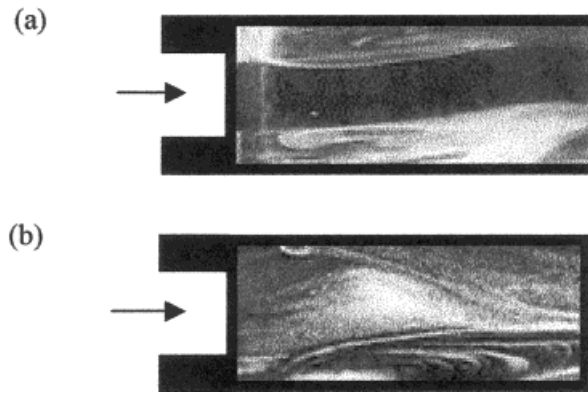


Figure 2. Flow visualization at (a) $Re = 600$, with smoke and light sheet visualization; (b) $Re = 20000$, with oil and pigment visualization.

profile different from the volume flow rate by less than 1%. Similar spanwise measurements in the downstream duct confirmed that the mean velocity was uniform over more than 80% of the span, as observed by Papadopoulos and Otugen [21], with volume flow rate obtained by integrating the measured velocity profiles at 70 step heights downstream less than 15% different from that obtained from the rotameter.

The mean velocity profiles of Figure 3 are asymmetric with two unequal reattachment lengths on the top and bottom wall. Reattachment lengths, normalized with the step height of the upstream duct, were deduced from the near-wall velocities to be equal to 17 and 3.4. Abbot and Kline [5] obtained reattachment lengths of 12 and 3.3, and Mehta [7] 15 and 4.4 step heights, but there is some uncertainty in all these values since they involve interpolation or observation of tufts. However, the differences in the dimensions of the two recirculating zones are evident and the probability of a ratio of recirculation lengths close to an odd integer as suggested by Cherdron *et al.* [2] is high. The profile in the exit plane was nearly symmetric, at which distance the potential region has disappeared. The maximum measured negative value is around $-0.2U_0$ and, after reattachment on the top wall the flow started to recover, although the velocity profile remained asymmetric at $x/h = 20$.

The r.m.s velocity profiles of Figure 4 are initially symmetric with a low turbulence intensity core and peaks located inside the separating shear layers at locations that correspond to the maximum mean velocity gradients. From a distance of $x/h = 3$ and on the lower half, the maximum and the low intensity core moved towards the bottom wall. On the upper half, the location of the local r.m.s maximum moved towards the centreline, where the vertical width of the region of high turbulence intensity increases with shear layer growth. As expected, turbulent diffusion caused the profiles to become more uniform with distance but without achieving symmetry by $x/h = 20$, at which the turbulence intensity was still equal to 10%, similar to that observed in single-sided plane expansions at around the same location, see Eaton and Johnston [22].

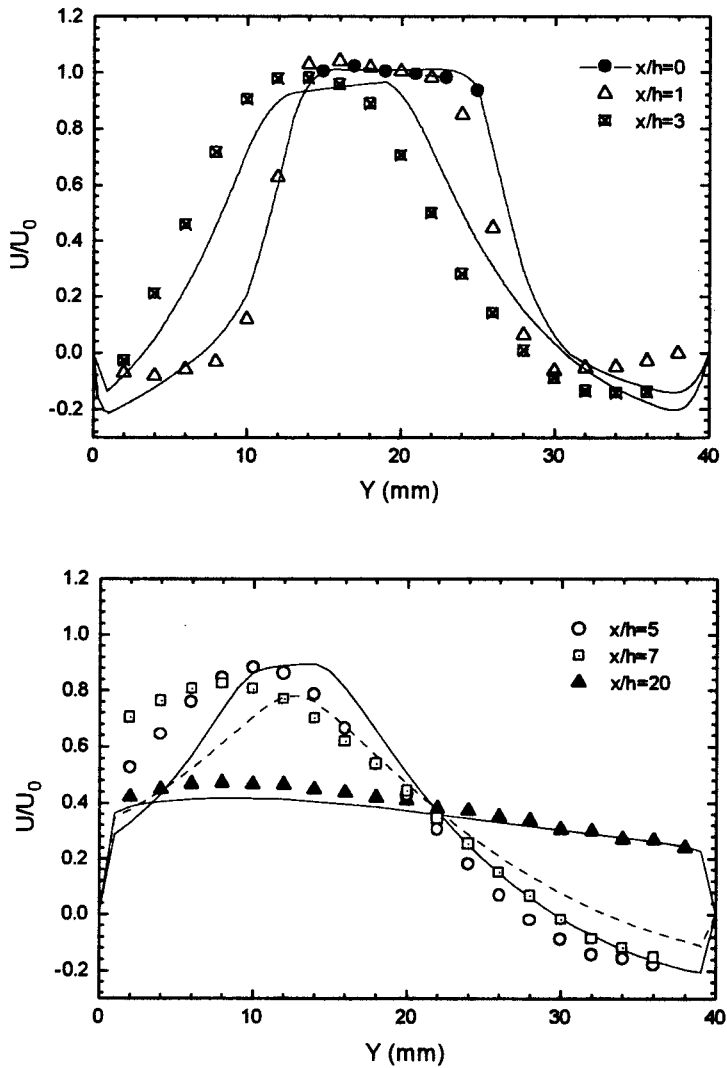


Figure 3. Mean axial velocity, $Re = 26500$, lines represent calculations.

4.2. Calculations

Calculations are presented first for laminar flows and compared with the measurements of Fearn *et al.* [3], who made use of area and aspect ratios of 3 and 8 respectively. With Reynolds numbers greater than 90, the flow was found to be asymmetric.

Figure 5 allows detailed comparison of the calculated and measured axial velocity profiles as a function of distance and for Reynolds numbers of 120 and 280, which were chosen to

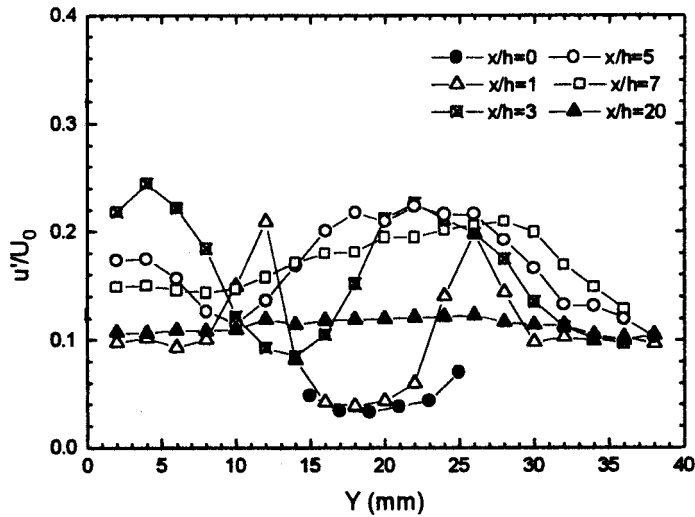


Figure 4. r.m.s axial velocity, $Re = 26500$.

highlight the two and three regions of recirculation. The profiles are initially highly skewed before returning to a plane Poiseuille flow, the agreement between the calculated and measured profiles is excellent for both Reynolds numbers, and the profile inside the third recirculation zone is accurately represented. The vector plots of Figure 6 illustrate the flow configuration with a Reynolds number of 280 with unequal recirculation zones adjacent to the step walls and a third separation zone on the same side as the shorter recirculation zone as the Reynolds number was increased.

The variation of reattachment length with Reynolds number is shown in Figure 7 for the three expansion ratios of Cherdron *et al.* [2], Fearn *et al.* [3] and Ouwa *et al.* [4]. The range of the Reynolds numbers for the three expansion ratios was chosen to avoid the need for three-dimensional calculations, which become necessary as the Reynolds number increases [2]. The reattachment location was determined as the position where the streamwise velocity was zero at the first grid point from the wall and the zero shear-stress location gave lengths that differed by less than 2%. The general trend for all expansion ratios displays a symmetric flow at low Reynolds numbers and, at a critical value, transition to asymmetric flow through a pitchfork bifurcation. At higher Reynolds numbers, both recirculation zones increased with the rate of change becoming more important with expansion ratio and a third recirculation zone appeared.

The parts of the curves that correspond to symmetric flow may be extrapolated to a finite recirculation length at zero Reynolds number and should correspond to the length of Moffat eddies [14]. Ouwa *et al.* [4] reported variations of the two first reattachment lengths (x_{r1} and x_{r2}) with Reynolds number and their results agree remarkably well with the present calculations. Figure 7 indicates calculated critical Reynolds numbers of 180, 90 and 45 for the

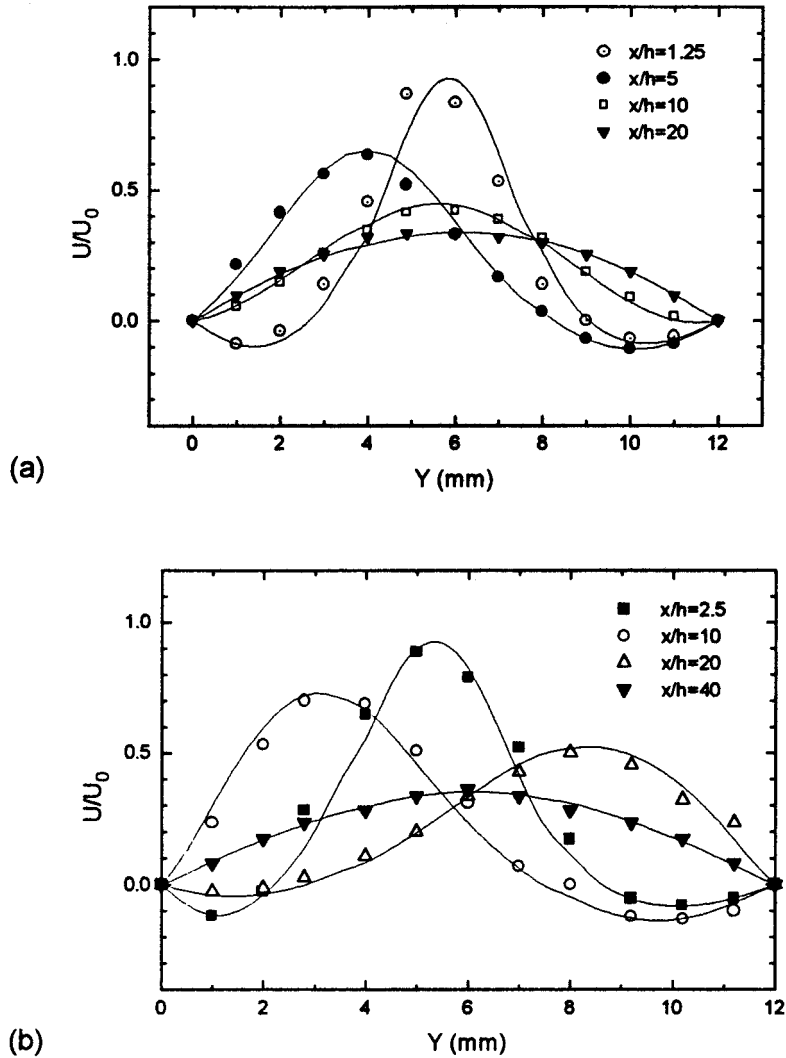


Figure 5. Axial mean velocity (Fearn *et al.*); (a) $Re = 120$, (b) $Re = 280$.

expansion ratios of 2, 3 and 5 respectively and these compare well with the measured results of 185, 88 and 45. From the same figure one can also observe that for an expansion ratio of 5, the third recirculation zone appears around a Reynolds number of 68, which compares well with the value of Ouwa *et al.* [4] of 75. Any differences are due to the presence of physical perturbations inevitably present in the geometry and experimental uncertainties. They are also in good agreement with the calculated results of Shapira *et al.* [23], Battaglia *et al.* [10] and Alleborn *et al.* [14]. The minor discrepancies from previous calculated results can be explained

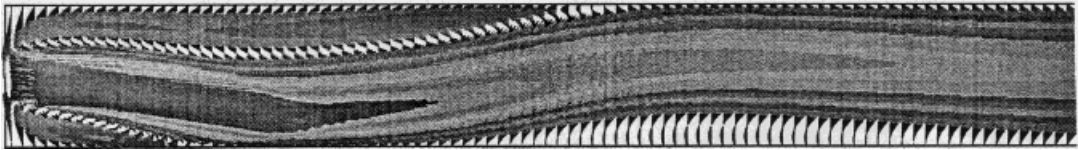


Figure 6. Vector plots for $Re = 280$, flow of Fearn *et al.* [3] (only part of the computational domain shown).

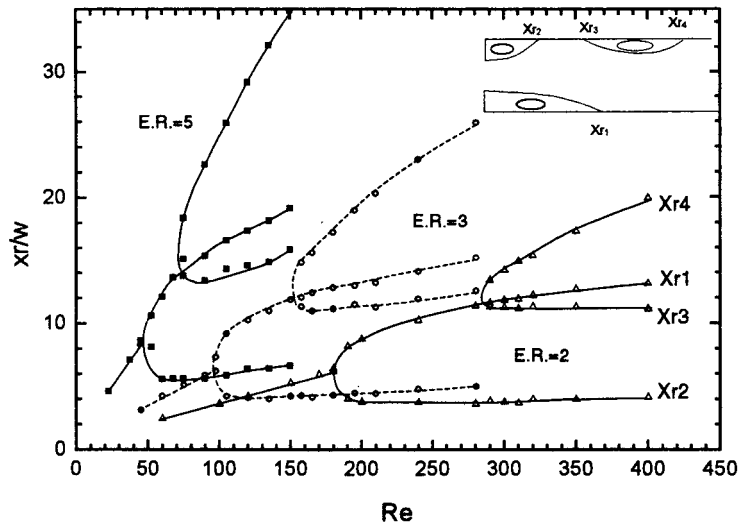


Figure 7. Reattachment lengths versus Reynolds number for expansion ratios of 2, 3 and 5.

readily in terms of the difficulty in obtaining an exact value for the transitional Reynolds number and the different computational techniques. It has been advocated that the bifurcation is due to truncation and rounding errors in the numerical calculations [13] but steady state simulations always return symmetry even if the whole flow domain is considered, as found in the present investigation. Thus, the asymmetric solution results from an unsteady phenomenon and the reality that symmetric solutions of the time-dependent equations become unstable beyond critical Reynolds numbers as demonstrated by Sobey and Drazin [24]. The effect of the boundary layer thickness on the reattachment lengths was examined for laminar flow in a single expansion ratio with one Reynolds number and showed that thin inlet boundary layers resulted in slightly (less than 10%) shorter reattachment lengths than fully developed inlet flow.

Figure 8 shows the velocity component normal to the symmetry line and measured on the centreline of the flow domain at a distance 25.5 mm from the expansion plane, for one of the flows of Fearn *et al.* [3]. It illustrates the appearance of asymmetry and bifurcation so that, at

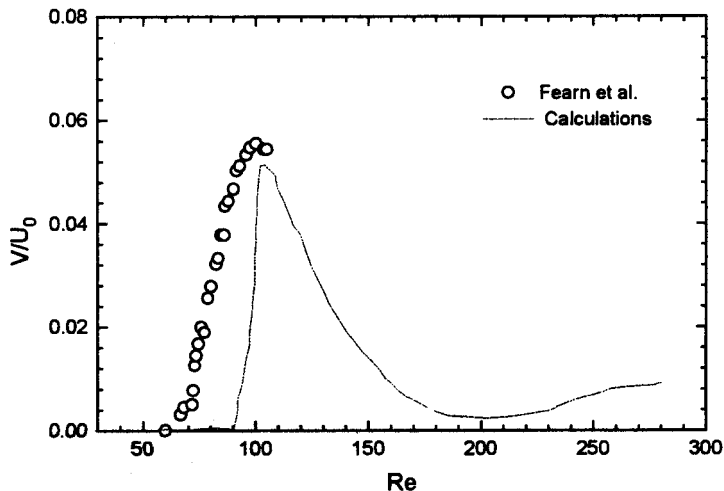


Figure 8. V velocity on centreline at 25.5 mm from expansion plane.

Reynolds numbers below the critical value, this velocity is zero and becomes finite as the flow becomes asymmetric, which occurs at a Reynolds number around 60. It can also be observed that the experimental Reynolds number is lower than the calculated one as observed by Fearn *et al.* [3].

The influence of the thickness of the separating boundary layer was considered with reference to the geometry of Fearn *et al.* [3] and for a Reynolds number based on the bulk velocity of 187, for fully developed and developing flow. The calculations revealed that the thinner boundary layer yielded reattachment lengths of $x_{r1}/h = 12.7$, $x_{r2}/h = 3.9$, $x_{r3}/h = 10.6$ and $x_{r4}/h = 19.4$, which compare with the values of 15.2, 5, 12.6 and 26 for the fully developed profile. It is also evident from Figure 9, which illustrates the velocity profiles downstream of the expansion plane, that the developing boundary layer results in thicker and shorter recirculation zones. Thus, the boundary layer thickness affects the shape and the length of the recirculation zones.

Spectrum analysis of the axial velocity component at several downstream locations, for expansion ratios of 2 and 3, belonging to the studies of Cherdron *et al.* [2] and Fearn *et al.* [3] and corresponding to Reynolds numbers where shedding was observed, did not reveal dominant frequencies and this suggests that two-dimensional simulations cannot fully represent this unsteadiness. It is of note that both references attribute the appearance of shedding to three-dimensional disturbances and the present results tend to confirm that three-dimensional effects are required to trigger vortex-like shedding. Since the Reynolds numbers involved are relatively low, three-dimensional direct numerical simulation (DNS) may confirm this suggestion.

The mean axial velocities for the turbulent flow are shown in Figure 3, with two main unequal recirculation zones. The general trend of the profiles is captured by the calculations,

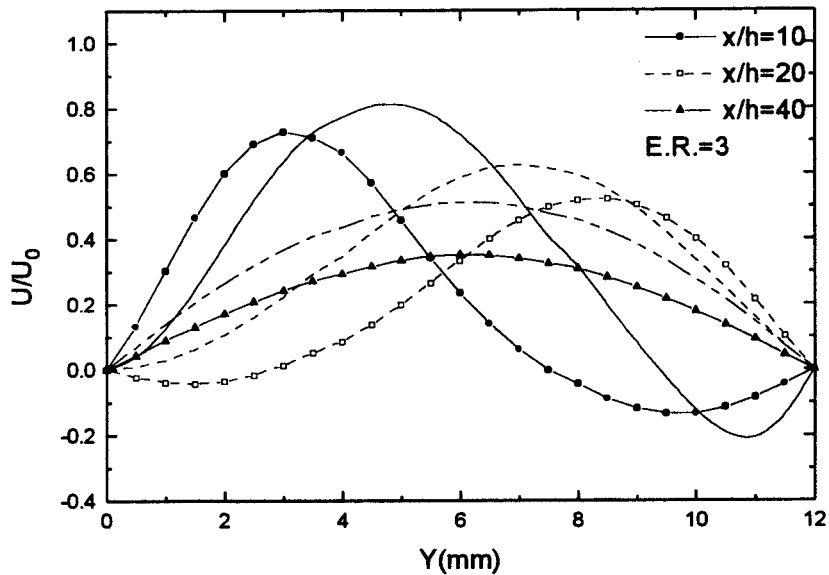


Figure 9. Profiles for different inlet boundary layer thickness—profiles with symbols relate to a fully developed laminar inlet flow.

but the cross-stream locations of maximum velocities are less well represented, e.g. at $x/h = 5$ and 7, and this suggests that the predicted high velocity region follows a different trajectory than that of the measurements with the measured flow impinging sooner. The negative velocities inside the recirculation regions are overpredicted and there is a tendency for the calculated profiles to recover more rapidly in part due to the use of the law of the wall as confirmed by the recent DNS of Le *et al.* [18] and the experiments of Jovic and Driver [25]. Further, the use of a two-layer model will not guarantee a better performance, since it has been reported that conflicting results have been obtained for backward-facing step flows by Chen and Patel [26] and Iacovides and Launder [27], who predicted the velocity profiles for a 1.125 expansion with a good accuracy, whereas for an expansion ratio of 1.5, Smyth [28] predicted a much stronger reverse flow than the experiments. Also, the results in the redevelopment region are sensitive to those obtained in the recirculation regions, where it is known that excessive diffusion in the shear layer is predicted by the present turbulence model. These model deficiencies are real but the high Reynolds number $k-\epsilon$ turbulence model remains still a representative model invariably used in engineering calculations.

The predicted pressure distribution on both walls is shown in Figure 10 and helps capture the gross dynamical features of the flow with the pressure inside the smaller recirculation zone much lower than in the larger. The absence of communication between the two regions makes possible the establishment of stable asymmetric flow, which would not have existed in axisymmetric sudden-expansion flows [29]. The distribution on the lower wall progresses in a manner similar to that found in backward-facing steps and that on the top wall presents a

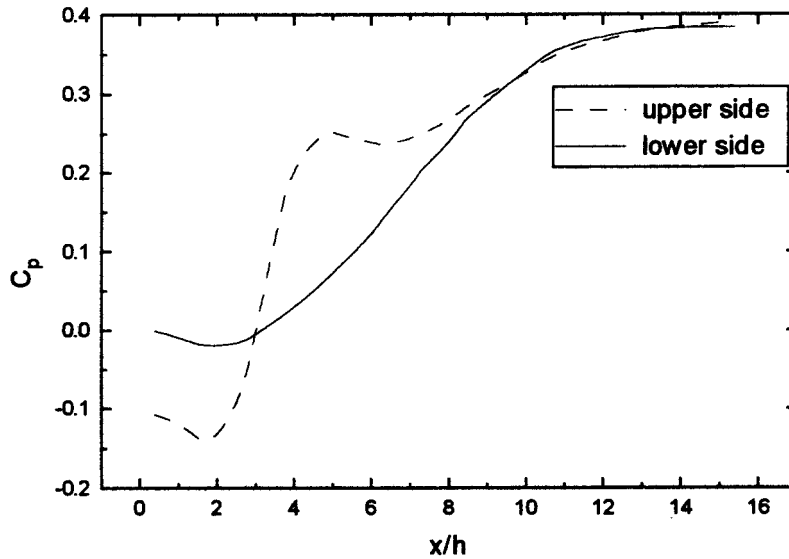


Figure 10. Pressure distribution on lower and upper walls at $Re = 26000$.

minimum at $x/h = 6.5$, which exists because the high velocity core stream impinged on the wall at that location. Thereafter, the pressure recovers to become identical to that on the opposite wall at $x/h = 12$.

The predicted reattachment lengths were equal to 3.85 and 10.7 step heights, in contrast to experimental values of 3.4 and 17. The discrepancy between the calculated and measured lengths of the shorter recirculation zone is modest, while that for the longer zone is significant. However, both the experimental and calculated ratios of reattachment lengths, 5 and 2.8 respectively, confirm the suggestion of Cherdron *et al.* [2], that the ratio should be close to an odd integer. The shorter reattachment length is more controlled by the pressure inside the recirculation bubble, as seen in Figure 10, and the Coanda effect, which competes with the spreading of the separating shear layer and deflects the core towards the wall. The longer reattachment length is less controlled by the pressure, with low values as in Figure 10, and more by diffusion. The calculated levels of turbulent diffusivity confirm this assertion, since important levels of eddy viscosity are associated with the shear layer corresponding to the longer recirculation zone. The $k-\varepsilon$ model is known to overpredict the generation of turbulent kinetic energy inside a separating shear layer and hence, its spreading rate which results eventually in a shorter reattachment length, as observed here and also by virtually all previous studies related however to flows behind single steps. Calculations were also performed with the same Reynolds number as that of the present experiment to assess the variation of reattachment lengths with expansion ratios. Figure 11 illustrates this in comparison with the mean lines of the flow visualization results of Abbot and Kline [5], where it can be seen that agreement is good. This is as much as can be said and caution has to be exercised when inferring definite conclusions from this figure, since the experimental data is based on crude visual observations.

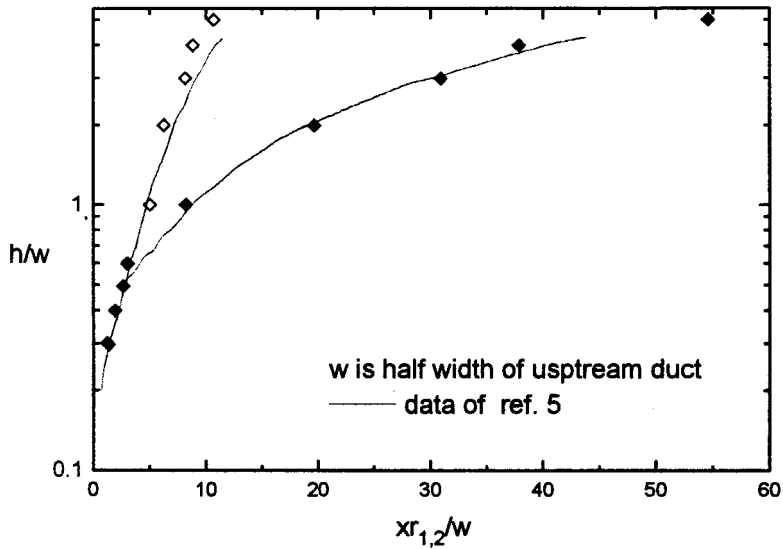


Figure 11. Reattachment length versus expansion ratio for $Re = 26000$.

Contours of the predicted turbulence kinetic energy are depicted in Figure 12, which shows a low energy skewed core extending from the plane of the step to $x/h = 6$. Turbulence kinetic energy is generated at different rates inside the separating shear layers and transported to other regions by diffusive action. It can be observed that most of the turbulent kinetic energy is

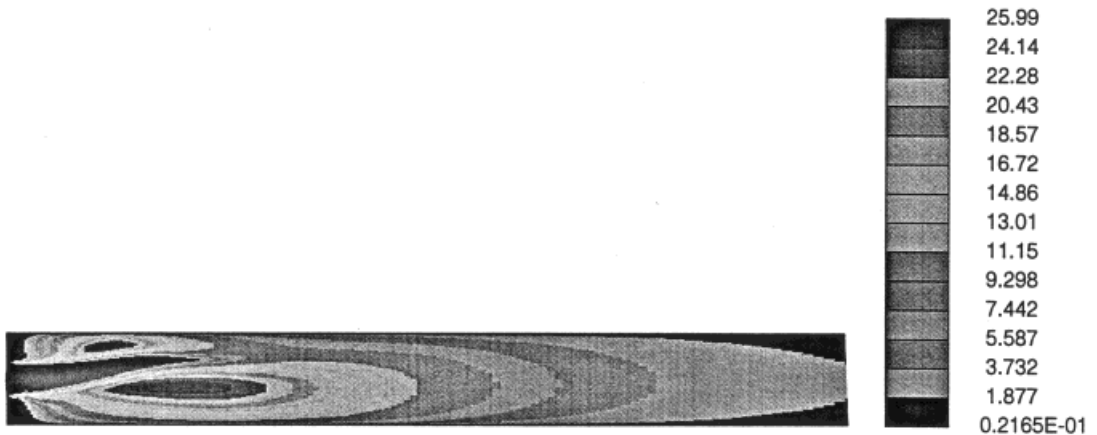


Figure 12. Contours of turbulent kinetic energy and eddy viscosity.

associated with the longer reattaching shear layer with different implications for the redevelopment of the boundary layers on the top and bottom walls.

5. CONCLUSIONS

The following conclusions can be extracted from this study:

It has been shown, by comparison with measurements, that the velocity, the reattachment lengths and the critical Reynolds number of laminar flows through plane sudden-expansions can be predicted by the present calculation method with excellent accuracy. The calculations also showed that the thickness of the inlet boundary layers affects the lengths and shape of the downstream recirculation bubbles, with thinner developing boundary layers yielding thicker and shorter bubbles.

The two-dimensional calculation method was unable to represent the shedding phenomena of laminar sudden-expansion flows at moderate Reynolds numbers and this tends to confirm previous conjectures that the phenomena are associated with three-dimensional disturbances. Three-dimensional DNS may provide further information.

New velocity measurements have been presented for turbulent sudden-expansion flows and used to appraise the calculation method. The trends of the measurements were represented by the calculations with detailed discrepancies, which included shortening of the longer reattachment length, larger reverse-flow velocities and a central jet with a trajectory slightly different from that of the measurements. The discrepancies were attributed mainly to the limitations of the $k-\varepsilon$ model, particularly in the presence of streamline curvature and anisotropic turbulence. The effect of the expansion ratio on the reattachment lengths was well represented.

REFERENCES

1. F. Durst, A. Melling and J.H. Whitelaw, 'Low Reynolds number flow over a plane symmetric sudden expansion', *J. Fluid Mech.*, **64**, 111–128 (1974).
2. W. Cherdron, F. Durst and J.H. Whitelaw, 'Asymmetric flows and instabilities in symmetric ducts with sudden expansions', *J. Fluid Mech.*, **84**, 13–31 (1978).
3. R.M. Fearn, T. Mullin and K.A. Cliffe, 'Nonlinear flow phenomena in a symmetric sudden expansion', *J. Fluid Mech.*, **211**, 595–608 (1990).
4. Y. Ouwa, M. Watanabe and H. Asawo, 'Flow visualisation of a two-dimensional water jet in a rectangular channel', *Jpn. J. Appl. Phys.*, **20**, 243–247 (1981).
5. D.E. Abbot and S.J. Kline, 'Experimental investigation of subsonic turbulent flow over single and double backward facing steps', *J. Basic Eng. Trans. ASME D*, **84**, 317–325 (1962).
6. A. Restivo and J.H. Whitelaw, 'Turbulence characteristics of the flow downstream of a symmetric plane sudden expansion', *J. Fluids Eng. Trans. ASME*, **100**, 308–310 (1978).
7. P.R. Mehta, 'Separated flow through large sudden expansions', *J. Hydraul. Div. ASCE*, **107**, 451–460 (1981).
8. F. Aloui and M. Souhar, 'Experimental study of two-phase bubbly flow in a flat duct symmetric sudden expansion—Part II', *Int. J. Multiphase Flow*, **22**, 849–861 (1996).
9. F. Durst, J.F.C. Pereira and C. Tropea, 'The plane symmetric sudden-expansion flow at low Reynolds numbers', *J. Fluid Mech.*, **248**, 567–581 (1993).
10. F. Battaglia, S.J. Tavener, A.K. Kulkarni and C.L. Merkle, 'Bifurcation of low Reynolds number flows in symmetric channels', *AIAA J.*, **35**, 99–105 (1997).
11. Y. Gagnon, A. Giovannini and P. Hebrard, 'Numerical simulation and physical analysis of high Reynolds number recirculating flows behind sudden expansions', *Phys. Fluids*, **A5**, 2377–2389 (1993).

12. J. Mizushima, H. Okamoto and H. Yamagushi, 'Stability of flow in a channel with a suddenly expanded part', *Phys. Fluids*, **8**, 2933–2942 (1996).
13. E.A. Foumeny, D.B. Ingham and A.J. Walker, 'Bifurcations of incompressible flow through plane symmetric channel expansions', *Comput. Fluids*, **25**, 335–351 (1996).
14. N. Alleborn, K. Nandakumar, H. Raszillier and F. Durst, 'Further contributions on the two-dimensional flow in a sudden expansion', *J. Fluid Mech.*, **330**, 169–188 (1997).
15. B.P. Leonard, 'A stable and accurate convective modeling procedure based on quadratic upstream interpolation', *Comput. Methods Appl. Mech. Eng.*, **19**, 59–98 (1979).
16. R.I. Issa, 'Solution of the implicitly discretised fluid flow equations by operator splitting', *J. Comput. Phys.*, **62**, 66–82 (1996).
17. R.D. Richtmeyer and K.W. Morton, *Difference Methods for Initial-Value Problems*, 2nd edn, Wiley-Interscience, New York 1967.
18. H. Le, P. Moin and J. Kim, 'Direct numerical simulation of turbulent flow over a backward-facing step', *J. Fluid Mech.*, **330**, 349–374 (1997).
19. W.J. Yanta and R.A. Smith, 'Measurements of turbulence transport properties with a laser Doppler velocimeter', *AIAA Paper 78-169*, 11th Aerospace Science Meeting, Washington, 1978.
20. F. Durst, A. Mellling and J.H. Whitelaw, *Laser Doppler Anemometry Principles and Practice*, Academic Press, New York, 1981.
21. G. Papadopoulos and M.V. Otugen, 'Separating and reattaching flow structure in a suddenly expanding rectangular duct', *J. Fluids Eng. Trans. ASME*, **117**, 17–23 (1995).
22. J.K. Eaton and J.P. Johnston, 'A review of research on subsonic turbulent flow reattachment', *AIAA J.*, **19**, 1093–1100 (1981).
23. M. Shapira, D. Degani and D. Weihs, 'Stability and existence of multiple solutions for viscous flow in a suddenly enlarged channels', *Comput. Fluids*, **18**, 239–258 (1990).
24. I.J. Sobey and P.G. Drazin, 'Bifurcations of two-dimensional channel flows', *J. Fluid Mech.*, **171**, 263–287 (1986).
25. S. Jovic and D.M. Driver, 'Backward-facing step measurements at low Reynolds number', *NASA Technical Memo 108807*, 1994.
26. H.C. Chen and V.C. Patel, 'Near-wall turbulence models for complex flows including separation', *AIAA J.*, **26**, 641–648 (1988).
27. H. Iacovides and B.E. Launder, 'The numerical simulation of flow and heat transfer in tubes in orthogonal rotation', *Proc. 6th Symp. on Turbulent Shear Flows*, Toulouse, France, 1990.
28. R. Smyth, 'Turbulent flow over a plane symmetric sudden expansion', *J. Fluids Eng.*, **101**, 348–353 (1979).
29. L. Khezzar, J.H. Whitelaw and M. Yianneskis, 'Round sudden expansion flows', *Proc. Inst. Mech. Eng.*, **200**, 6–13 (1986).